Model for convection in binary liquids

St. Hollinger, M. Lücke, and H. W. Müller

Institut für Theoretische Physik, Universität des Saarlandes, Postfach 151150, D–66041 Saarbrücken, Germany
(Received 17 September 1997)

A minimal, analytically manageable Galerkin type model for convection in binary mixtures subject to realistic boundary conditions is presented. The model elucidates and reproduces the typical bifurcation topology of extended stationary and oscillatory convective states seen for negative Soret coupling: backwards stationary and Hopf bifurcations, saddle node bifurcations to stable strongly nonlinear stationary and traveling wave (TW) states, and merging of the TW solution branch with stationary states. Also unstable standing wave solutions are obtained. A systematic analysis of the concentration balance for liquid mixture parameters has led to a representation of the concentration field in terms of two linear and two nonlinear modes. This truncation captures the important large-scale effects in the laterally averaged concentration field resulting from advective and diffusive mixing. Also the fact that with increasing flow intensity along the TW solution branch the frequency decreases monotonically in the same way as the mixing increases—the variance of the concentration distribution decreases—is ensured and reproduced well. Universal scaling relations between flow intensity, frequency, and variance of the concentration distribution (degree of mixing) in a TW are predicted by the model and have been confirmed by numerical solutions of the full equations. The validity of the model is checked by comparison with numerical solutions of the full field equations. [S1063-651X(98)08804-7]

PACS number(s): 47.20.−k, 47.10.+g, 03.40.Gc

I. INTRODUCTION

A great deal of effort has recently been undertaken to investigate convection in binary fluid mixtures as an example for pattern formation far from equilibrium [1]. This system provides an experimentally convenient device [2–12] with a well established theoretical description [13,14] allowing quantitative comparisons of theoretical investigations [15–29] with experiments. For a review and additional references, see [1,18]. Compared to convection in ordinary one-component fluids the spatiotemporal properties are far more complex due to the influence of Soret sustained concentration gradients. The evolution of the concentration field is governed by the interplay of typically strong nonlinear convective transport and mixing, weak dissipative solutal diffusion, and the Soret effect [1,13,14]. The latter is a source of concentration fluctuations. It generates concentration gradients in response to the externally applied temperature difference and to local temperature gradients. The strength of the Soret coupling is measured by the dimensionless separation ratio ψ [1,13,14].

The concentration field changes the convective dynamics via solutal buoyancy forces entering into the momentum balance. In this way concentration gradients directly influence the flow which in turn changes and mixes the concentration. In binary liquids, this strongly nonlinear feedback is only weakly damped by small diffusive homogenization so that the concentration field distribution shows significant anharmonic and boundary layer structures. It is, however, the existence of the feedback loop that ultimately causes convection in binary mixture to exhibit such a rich variety of patterns arising from stationary and oscillatory [30] instabilities: Depending on the parameters the hydrodynamic balance equations show convective solutions that bifurcate out of the quiescent conductive basic state in the form of (i) straight, stationary, parallel rolls, (ii) traveling waves (TWs) consist-

ing of propagating rolls, (iii) standing wave (SW) oscillations, and (iv) stationary squares. Besides these primary states, there are close to onset of convection pulselike, spatially localized traveling wave (LTW) states consisting of only a few TW rolls, oscillating square patterns [31], cross-roll structures [32], and also (spiral) defect chaos [33].

In the present paper the focus is on two-dimensional (2D) spatially extended convective structures consisting of straight parallel rolls that occur at negative separation ratios $-0.6 < \psi < 0$. For typical fluid parameters convection arises via an oscillatory subcritical bifurcation. The emerging solution branch locates unstable TWs that are "weakly nonlinear" only near the onset. These unstable waves become strongly nonlinear and anharmonic [20,34] well before the occurrence of a saddle node at which they are stabilized on an upper solution branch. Simultaneously, the TW propagation speed slows down from its large value at the Hopf bifurcation threshold towards zero at the final transition to steady overturning convection (SOC). There, the amplitude of the concentration wave vanishes since in the SOC state the fluid is well mixed to a mean concentration level except within narrow boundary layers. This SOC state is somewhat similar to the convective rolls in one-component fluids.

The bifurcation topology described above has been verified by several experimental groups (e.g., [3]; for additional references see [1,18]). A detailed insight into the spatiotemporal variations of TW and SOC states along their upper solution branches and their parameter dependence provided numerical simulations of Barten *et al.* [15,18]. A quantitative description of the whole bifurcation branches [20,34] including the lower branches that were unavailable to Barten *et al.* was obtained recently with a multimode Galerkin (MMG) expansion including several hundred modes. The MMG predictions agree very well [20,34] with results from finite difference marker and cell (MAC) simulations of the full field

equations supplemented by a control process which allows us to evaluate also unstable TW and SOC states [35].

Since the first observations of TWs, much theoretical research activity has been devoted to developing an understanding and to developing models for these phenomena. Based upon an earlier few-mode Galerkin model [26] Cross [36] and also Ahlers and Lücke [37] investigated Soret-driven convection with permeable boundary conditions. They found TW states only locally at the onset of convection since for permeable conditions the onset of TW convection is tricritical. Linz *et al.* [24] implemented impermeable conditions yielding a subcritical primary bifurcation to TWs. This observation is in agreement with small amplitude computations of Schöpf and Zimmermann [25]. Both approaches, however, do not explain the stabilization of the TW branch via a saddle node bifurcation. Bensimon *et al.* [19] considered the case of weak Soret coupling by means of a small-ψ expansion treating the concentration field numerically. They observed a stable TW branch and interpreted the TW-SOC transition as a boundary layer induced instability. Due to the expansion in ψ and due to the weak diffusion limit the application range in fluid parameter space is rather narrow [38].

The detailed numerical analyses [15,18,20,34,39] elucidating the influence of the spatiotemporal behavior of the concentration field on various properties of TW states, e.g., on the variation of flow amplitude, frequency, and mixing with heating rate have clearly shown that the success of a model description sensitively hinges upon the representation of the concentration field. It has to capture the essence of the spatiotemporal structures following from the combined action of strong nonlinear advection and weak diffusion on the one hand and the generation of Soret induced concentration currents by temperature gradients on the other hand. A model that reproduces with few degrees of freedom all essentials of the bifurcation behavior of flow amplitude, frequency, and mixing is presently not available—neither in the form of coupled amplitude equations nor in Galerkin type form. The respective reasons for their deficiencies are discussed in the text.

The present paper aims at filling this gap. We present a few-mode Galerkin model which rests upon a careful analysis [34,39] of the concentration balance in liquid mixtures and explains among others the whole TW solution branch from oscillatory onset up to its merging with the upper SOC branch and the associated changes in the spatiotemporal structure of the states.

We introduce the system and formulate the theoretical task in Sec. II. In Sec. III we construct the Galerkin model and give a detailed account of how the concentration field is represented. The main body of the paper (Sec. IV) is dedicated to an extensive discussion of the results. Wherever possible we provide analytic expressions for characteristic quantities like thresholds, bifurcation points, and order parameters like convective amplitude, frequency, heat flux, and variance of the concentration distribution. The SOC and TW states will be compared in quantitative detail with simulations. Our model also yields unstable SW solutions.

II. SYSTEM

We consider a convection cell of height d. It contains a binary fluid of mean temperature $\bar{T}$ and mean concentration $\bar{C}$ of the lighter component confined between two perfectly heat conducting and impervious plates. This setup is exposed to a vertical gravitational acceleration g and to a vertical temperature gradient $\Delta T/d$ directed from top to bottom. The fluid has a density ρ which varies due to temperature and concentration variations governed by the linear thermal and solutal expansion coefficients $\alpha = -(1/\rho)(\partial \rho/\partial \bar{T})$ and $\beta = -(1/\rho)(\partial \rho/\partial \bar{C})$, respectively. Its viscosity is ν, the solutal diffusivity is D, and the thermal diffusivity is κ. The thermodiffusion coefficient k_T quantifies the Soret coupling which describes the change of concentration fluctuations due to temperature gradients.

The vertical thermal diffusion time is used as the time scale d^2/κ of the system and velocities are scaled by κ/d. Temperatures are reduced by the temperature difference ΔT across the layer and concentration deviations from the mean concentration by $(\alpha/\beta)\Delta T$. The scale for the pressure is given by $\rho \kappa^2/d^2$. Then, the balance equations for mass, momentum, heat, and concentration [13,14] read in Oberbeck-Boussinesq approximation [40,18]

$$0 = -\nabla \cdot \mathbf{u}, \tag{2.1a}$$

$$\partial_t \mathbf{u} = -(\mathbf{u} \cdot \nabla)\mathbf{u} - \nabla\left[p + \left(\frac{d^3}{\kappa^2}g\right)z\right] + \sigma \nabla^2 \mathbf{u} + R\sigma(T+C)\mathbf{e}_z, \tag{2.1b}$$

$$\partial_t T = -\nabla \cdot \mathbf{Q} = -\nabla \cdot [\mathbf{u}T - \nabla T], \tag{2.1c}$$

$$\partial_t C = -\nabla \cdot \mathbf{J} = -\nabla \cdot [\mathbf{u}C - L\nabla(C - \psi T)]. \tag{2.1d}$$

Here, the currents of heat and concentration, $\mathbf{Q}$ and $\mathbf{J}$, respectively, are introduced and T and C denote deviations of the temperature and concentration fields, respectively, from their global mean values $\bar{T}$ and $\bar{C}$. The Dufour effect [40,41] that provides a coupling of concentration gradients into the heat current $\mathbf{Q}$ and a change of the thermal diffusivity is discarded in Eq. (2.1c) since it is relevant only in few binary gas mixtures [6] and in liquids near the liquid-vapor critical point [22].

Besides the Rayleigh number $R = (\alpha g d^3/\nu\kappa)\Delta T$ measuring the thermal driving of the fluid there enter three additional numbers into the field equations (2.1a)–(2.1d): the Prandtl number $\sigma = \nu/\kappa$, the Lewis number $L = D/\kappa$, and the separation ratio $\psi = -(\beta/\alpha)(k_T/\bar{T})$. The latter characterizes the sign and the strength of the Soret effect. Negative Soret coupling ψ induces concentration gradients antiparallel to temperature gradients. In this situation, the buoyancy induced by solutal changes in density is opposed to the thermal buoyancy. When the total buoyancy exceeds a threshold, convection sets in, typically in the form of straight rolls for negative ψ. Ignoring field variations along the roll axes we describe henceforth 2D convection in an x-z plane perpendicular to the roll axes.

Form and strength of convection and its influence on convective concentration and temperature transport are measured by the following order parameters. (i) The maximum w_{max} of the vertical velocity field. (ii) The Nusselt number $N = \langle \mathbf{Q} \cdot \mathbf{e}_z \rangle_x$ giving the lateral average of the vertical heat current through the system. In the basic state of quiescent

heat conduction its value is 1 and larger than 1 in all convective states. (iii) The variance

$$M = \sqrt{\langle C^2 \rangle_{x,z} / \langle C_{\text{cond}}^2 \rangle_{x,z}} \qquad (2.2)$$

of the concentration field being a measure for the mixing in the system. The better the fluid is mixed the more the concentration is globally equilibrated to its mean value 0— optimally mixed, strongly convecting states force M to vanish. In the conductive reference state denoted by the subscript ''cond'' the vertical Soret induced concentration gradient gives rise to a variance of $\sqrt{\langle C_{\text{cond}}^2 \rangle_{x,z}} = |\psi| / \sqrt{12}$. (iv) The frequency ω of a TW. Thus extended TWs with a wave number k have a phase velocity $v = \omega / k$. They are stationary states in a reference frame comoving with v relative to the laboratory system.

The solution of the partial differential equations (2.1a)–(2.1d) requires boundary conditions for the fields. We use realistic no slip conditions for the top and bottom plates at $z = \pm 1/2$,

$$\mathbf{u}(x, z = \pm 1/2; t) = \mathbf{0},$$

and assume perfect heat conducting plates by

$$T(x, z = \pm 1/2; t) = \mp 1/2.$$

Furthermore, impermeability for the concentration is guaranteed by

$$\mathbf{e}_z \cdot \mathbf{J} = -L\partial_z(C - \psi T)(x, z = \pm 1/2; t) = 0. \qquad (2.3)$$

We should like to stress again that we restrict ourselves to the description of extended roll-like patterns that are homogeneous in one lateral direction, say, y. So, we investigate 2D states of a certain lateral periodicity length $\lambda = 2\pi/k$. In most cases we take $k = \pi$, i.e., λ twice the thickness of the fluid layer, which is close to the critical wavelengths for the negative Soret couplings investigated here.

III. MODE SELECTION AND GALERKIN MODEL

A. Temperature and velocity fields

The temperature field consisting of a linear conductive profile $-z$ and a convective deviation is truncated by

$$T(x, z; t) = -z + T_{02}(t)\sqrt{2}\sin 2\pi z$$

$$+ [T_{11}(t)e^{-ikx} + \text{c.c.}]\sqrt{2}\cos \pi z \qquad (3.1)$$

as in the standard Lorenz model [42] and its first extensions to convection in binary mixtures with permeable [26,36,37] and impermeable boundaries [23,24,43]. These models do not provide a satisfactory representation of strongly nonlinear TW convection since they used a combination of concentration and temperature fields in order to fulfill the impermeability of the plates exactly without extending the temperature truncation adequately. For a discussion of this point see Ref. [34]. Here, we truncate the concentration itself. This approach avoids the necessity of a more complicated representation of the temperature field.

For the velocity field we adopt an earlier successful [34] one-mode description

$$w(x, z, t) = [w_{11}(t)e^{-ikx} + \text{c.c.}]\cos^2 \pi z. \qquad (3.2)$$

Equation (3.2) completes the Galerkin approximation of velocity and temperature in our model.

B. Selecting the concentration field modes

In order to select adequate concentration modes a detailed analysis of the concentration balance and field structure of SOC and TW states is necessary.

1. Lateral average of the concentration and deviation

The first step of our analysis is to decompose the concentration

$$C(x, z; t) = \langle C \rangle_x + (C - \langle C \rangle_x) =: C_0(z; t) + c(x, z; t) \qquad (3.3)$$

into its lateral mean $C_0(z; t)$ and the deviation $c(x, z; t)$ from it. Inserting this decomposition into the balance equation (2.1d) for the concentration and averaging it yields two coupled equations for C_0 and c,

$$\partial_t C_0 = -\partial_z \langle wc \rangle_x + L\partial_z^2 C_0, \qquad (3.4a)$$

$$(\partial_t + \mathbf{u} \cdot \nabla)c = \partial_z \langle wc \rangle_x - w\partial_z C_0 + L\nabla^2 c. \qquad (3.4b)$$

In both of these equations we have discarded the Soret coupling term $L\psi\nabla^2 T$ *in the bulk* of the fluid. However, the Soret coupling will not be dropped in the boundary condition (2.3). The motivation and justification for this approximation are discussed in quantitative detail in Ref. [34]. Here, we only mention that the basic justification is the smallness of the Lewis number L in liquids so that transport by diffusion and the Soret effect—both enter the balance with a weight L—are small compared with advection. In those regions where advection needs to be balanced by another transport mechanism strong concentration gradients are observed whereas the temperature gradient shows no such boundary layers. Thus, an adequate balance is assured by advection and diffusion and the additional concentration source or sink—the Soret effect—can be omitted in the bulk. Only in the impermeable boundary condition does the Soret effect lead to a sizable nonvanishing mean concentration gradient at the plates which cannot be ignored.

In a SOC fixed point and also in a TW the lateral average of the concentration field is temporally constant. Thus it can be calculated explicitly from Eq. (3.4a) to be

$$C_0(z) = -\psi Nz + \frac{1}{L}\int_0^z dz' \langle wc \rangle_x. \qquad (3.5)$$

Here, the impermeable boundary condition (2.3),

$$\partial_z C_0(\pm 1/2) = \psi \partial_z T_0(\pm 1/2) = -\psi N, \qquad (3.6)$$

relating the lateral averages C_0 and T_0 has been used in the first integration of Eq. (3.4a) from $-1/2$ to z. The second integration is taken from 0 to z since $C_0(z=0) = 0$ as required by the mirror glide symmetry $C(x+\lambda/2, z) = -C(x, -z)$ for SOC and TW states [15,18]. When describing TW as well as SOC fixed points the relation (3.5) can be inserted into the evolution equation (3.4b) giving

$$(\partial_t + \mathbf{u}\cdot\nabla)c = L\nabla^2 c + \psi N w + \left(\partial_z - \frac{w}{L}\right)\langle wc\rangle_x. \quad (3.7)$$

The solution c of this equation completely determines the relaxed TW and SOC concentration field whenever the vertical velocity field together with the Nusselt number is given. Just that is realized by the truncations for the velocity (3.2) and temperature (3.1) field in Sec. III A. With c, w, and N also the TW and SOC spatial structure of the lateral mean of the concentration is determined via Eq. (3.5). The last task is therefore to select modes for c that approximate the TW and SOC structure appropriately.

2. Symmetry decomposition and lateral mode truncation

The mode selection of c is based among others on the insight gained in Ref. [39] from a symmetry decomposition of c. The decomposition was realized [39] with respect to the different parities under the mirror operations $x\to -x$ and $z\to -z$ so that the four symmetry classes $\mathcal{S}^{++}$, $\mathcal{S}^{+-}$, $\mathcal{S}^{-+}$, and $\mathcal{S}^{--}$ are obtained. The first (second) superscript denotes the parity under the operation $x\to -x$ ($z\to -z$). In relaxed TWs and SOCs the lateral coordinate x can be combined with the time t to $x-vt$ so that the time derivatives in TWs can be replaced by $-v\partial_x$ and the argument t in the field c can be dropped. One main result of Ref. [39] was the observation that field components of the symmetry $\mathcal{S}^{--}$ are not needed for a quantitative description of the TW and SOC bifurcation topology and that the fields of the class $\mathcal{S}^{+-}$ are made up mainly by the zeroth lateral Fourier mode. Consequently, the SOC and TW concentration field c can be represented well by just two parts

$$c(x,z) = c^{++}(x,z) + c^{-+}(x,z) \quad (3.8)$$

belonging to the symmetry classes $\mathcal{S}^{++}$ and $\mathcal{S}^{-+}$. Using the approximation (3.8) for c one obtains from Eq. (3.7) two equations

$$-v\partial_x c^{-+} + \frac{1}{L}w\langle wc^{++}\rangle_x = N\psi w + L\nabla^2 c^{++}, \quad (3.9a)$$

$$-v\partial_x c^{++} = L\nabla^2 c^{-+} \quad (3.9b)$$

for the c^{++} and c^{-+} fields of fully relaxed SOCs and TWs. Here, the vertical velocity field w was fixed to belong to the symmetry class $\mathcal{S}^{++}$ in the *Ansatz* (3.2) by choosing the temporal phase adequately and then switching from x to $x-vt$. Furthermore, we used the fact that the application of the advective derivatives $u\partial_x$ and $w\partial_z$ to c^{++} and c^{-+} generate fields with negative vertical parity that do not belong to the two retained symmetry classes $\mathcal{S}^{++}$ and $\mathcal{S}^{-+}$ for c. The same holds also for $\partial_z\langle wc\rangle_x = \partial_z\langle wc^{++}\rangle_x$.

The important implication of Eqs. (3.9) is that the *lateral variation* of the concentration field $c(x,z)$ is restricted to $\sin kx$ and $\cos kx$ if one uses the approximations (3.8) and (3.2). The reason is that $w\langle wc^{++}\rangle_x$ as well as $N\psi w$ have the lateral variation of w, i.e., $\cos kx$, and no other inhomogeneity in Eq. (3.9) excites higher modes. We should like to stress that all these restrictions are based on a quantitative investigation of their implications. Thus they do not endanger the success of our model, as we will see below.
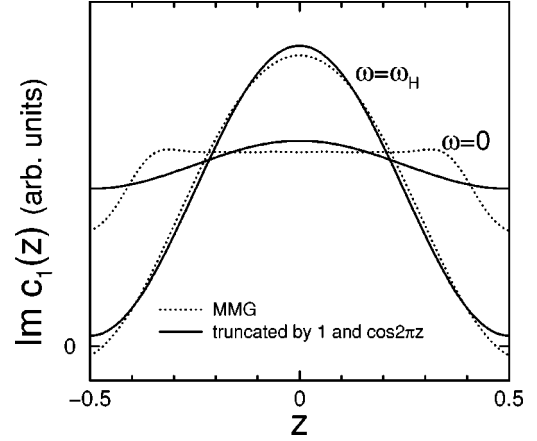
FIG. 1. Vertical profiles of that part of the first lateral Fourier mode of the concentration being in phase with the stream function (in our notation the imaginary part). Shown are the eigenfunctions at the Hopf bifurcation ($\omega = \omega_H$) and at the SOC-TW transition ($\omega = 0$) with arbitrary normalizations. Dots refer to a many-mode Galerkin scheme, solid lines to an optimal truncation by a linear combination of 1 and $\cos 2\pi z$. Parameters are $L=0.01$, $\sigma=10$, and $\psi = -0.25$.

3. Vertical variation

The last task is to select modes for the *vertical spatial dependence* of $c(x,z)$ in the form

$$c(x,z) = c_1(z)e^{-ikx} + \text{c.c.}, \quad (3.10)$$

with c_1 being the first lateral Fourier mode of c. Numerical calculations [18,34] have revealed that the main contribution to $c_1(z)$ is made up by a part being phase shifted by 90° with respect to the vertical velocity field. With the velocity *Ansatz* (3.2) and the choice that w_{11} is real, this implies that $c_1(z)$ is dominated by its imaginary part. This holds as long as the phase velocity v is large compared with the Lewis number $L = O(0.01)$.

The vertical spatial dependence of Im $c_1(z)$ is investigated in Fig. 1. Therein, we demonstrate that the "exact" solution (dotted line) obtained from a MMG scheme can very well be reproduced by a linear combination of 1 and $\cos 2\pi z$, i.e., of the first two modes with the boundary condition $\partial_z c = 0$ at $z = \pm 1/2$. This holds both for the bifurcation out of the heat conducting state ($\omega = \omega_H$) and for the SOC-TW transition ($\omega = 0$). The mode amplitudes of 1 and $\cos 2\pi z$ were optimally chosen in Fig. 1 in order to demonstrate the usefulness of the representation of the first lateral Fourier mode

$$c_1(z;t) = \sqrt{2}[c_{10}(t) + c_{12}(t)\cos 2\pi z] \quad (3.11)$$

in terms of 1 and $\cos 2\pi z$ with two complex amplitudes $c_{10}(t)$ and $c_{12}(t)$.

According to Eq. (3.5), the *spatial dependence* of the zeroth Fourier mode $C_0(z)$ can be calculated by integrating the product of $\cos^2\pi z$ for the vertical dependence of w with 1 and $\cos 2\pi z$, respectively, coming from c. This procedure leads to vertical modes of the form $(2\pi z + \sin 2\pi z)$ and $(-4\pi z + \sin 4\pi z)$. Their real amplitudes are labeled by c_{02} and c_{04}, respectively. These two modes c_{02} and c_{04} are con-

stant in SOC and TW fixed points. To derive a model that includes temporal variations of these modes as well, both modes are taken as time dependent.

The complete Galerkin *Ansatz* for the concentration field is therefore given by

$$\frac{C(x,z,t)}{-\psi} = \{1 + 2\pi\sqrt{2}[c_{02}(t) - 2c_{04}(t)]\}z$$

$$+ c_{02}(t)\sqrt{2}\sin 2\pi z + c_{04}(t)\sqrt{2}\sin 4\pi z$$

$$+ [c_{10}(t)e^{-ikx} + \text{c.c.}]\sqrt{2}$$

$$+ [c_{12}(t)e^{-ikx} + \text{c.c.}]\sqrt{2}\cos 2\pi z. \qquad (3.12)$$

In order to avoid the appearance of temperature modes in Eq. (3.12) we approximate the boundary condition (3.6) by $\partial_z C_0(\pm 1/2) = -\psi$ that deviates from the correct value by a factor equal to the Nusselt number $N = O(1)$. This approximation can be understood as the leading term in an amplitude expansion of N which starts at $N = 1$. The exact value of N is of minor importance in the boundary condition (3.6). Only the existence of a finite slope of C_0 at the plates is crucial.

Similarly, a lateral variation of the vertical derivative of C, i.e., of c, at the plates can be seen as a higher-order contribution that scales with the field amplitudes and not with $O(1)$. The reader can convince himself of the smallness of the derivatives of $\text{Im}c_1(z)$ at the plates in Fig. 1.

C. Galerkin model

1. Scalings

We use $r = R/R^0$ as control parameter. Here, $R^0 = \frac{1}{6}(3\pi/2)^6 \simeq 1825.14$ is the stability threshold of the quiescent heat conducting state of the pure fluid with respect to disturbances of a wave number $k = \pi$ within our model. This is not exactly the minimum of the marginal curve. It is calculated as $0.9998R^0$ at $k = 0.9827\pi$. But since we are not interested here in wave number dependencies we fix $k = \pi$.

The complex amplitudes of the first lateral Fourier modes, $f \in \{w_{11}, T_{11}, c_{10}, c_{12}\}$, are written in a vector notation

$$\mathbf{f} = (\text{Re}f, \text{Im}f)^T. \qquad (3.13)$$

We scale the mode amplitudes in the following way:

$$\mathbf{X} = \frac{8}{5\pi^2}\mathbf{w}_{11}, \qquad (3.14a)$$

$$\mathbf{Y} = \frac{6\pi\sqrt{2}}{5}r\mathbf{T}_{11}, \quad Z = \frac{6\pi\sqrt{2}}{5}rT_{02}, \qquad (3.14b)$$

$$\mathbf{U}_1 = \frac{32\sqrt{2}}{5}r\mathbf{c}_{10}, \quad \mathbf{U}_2 = \frac{32\sqrt{2}}{5}r\mathbf{c}_{12}, \qquad (3.14c)$$

$$V_1 = \frac{256\sqrt{2}}{15\pi}rc_{02}, \quad V_2 = \frac{256\sqrt{2}}{5\pi}rc_{04}. \qquad (3.14d)$$

Additionally, we introduce

$$\widetilde{\sigma} = \frac{27}{14}\sigma, \quad \tau = \frac{1}{2\pi^2}, \quad a = \frac{9\pi^2}{128} \simeq 0.6940. \qquad (3.14e)$$

2. Order parameters

The order parameters maximal convective amplitude w_{max}, Nusselt number N, and mixing number M can be expressed by

$$w_{\text{max}} = \frac{5\pi^2}{4}|\mathbf{X}|, \qquad (3.15a)$$

$$N = \int_{-1/2}^{1/2} dz \langle \mathbf{Q}\cdot\mathbf{e}_z\rangle_x = 1 + \frac{25}{18}\frac{1}{r}\mathbf{X}\cdot\mathbf{Y}, \qquad (3.15b)$$

$$M^2 = \frac{12}{\psi^2}\langle C^2\rangle_{x,z} = 1 + \frac{75}{128}\frac{1}{r^2}\left(|\mathbf{U}_1|^2 + \frac{1}{2}|\mathbf{U}_2|^2\right)$$

$$+ \frac{45}{64}\frac{1}{r}\left(1 + \frac{\pi^2}{3}\right)V_1 - \frac{15}{128}\frac{1}{r}\left(1 + \frac{4\pi^2}{3}\right)V_2$$

$$+ \frac{1125\pi^2}{32\,768}\frac{1}{r^2}\left(V_1 - \frac{1}{3}V_2\right)^2 + \frac{75\pi^4}{16\,384}\frac{1}{r^2}\left(V_1 - \frac{2}{3}V_2\right)^2.$$

$$(3.15c)$$

Here, the Nusselt number is computed as the global spatial average of the vertical heat flux since due to the truncation of velocity and temperature fields in different bases the laterally averaged vertical heat flux which is conventionally used for evaluating the Nusselt number has a slight z dependence. This problem occurs in all few-mode Galerkin approximations with no slip boundary conditions, see, e.g., [44,41].

3. Model

We insert the field truncations of Secs. III A and III B into the basic equations (2.1b)–(2.1d) without bulk Soret effect and scale the mode amplitudes according to Eqs. (3.14a)–(3.14d). Then, the following model for the convection in binary fluid mixtures is obtained:

$$\tau\dot{\mathbf{X}} = -\widetilde{\sigma}\left[\mathbf{X} - \mathbf{Y} + a\psi\left(\mathbf{U}_1 + \frac{1}{2}\mathbf{U}_2\right)\right], \qquad (3.16a)$$

$$\tau\dot{Z} = -2(Z - \mathbf{X}\cdot\mathbf{Y}), \qquad (3.16b)$$

$$\tau\dot{\mathbf{Y}} = -\mathbf{Y} + \mathbf{X}(r - Z), \qquad (3.16c)$$

$$\tau\dot{V}_1 = -\frac{6L}{5}V_1 - \frac{32L}{15}V_2 + \mathbf{X}\cdot\left(\mathbf{U}_1 + \frac{7}{3}\mathbf{U}_2\right), \qquad (3.16d)$$

$$\tau\dot{V}_2 = -\frac{6L}{5}V_1 - \frac{24L}{5}V_2 + \mathbf{X}\cdot(\mathbf{U}_1 + 4\mathbf{U}_2), \qquad (3.16e)$$

$$\tau\dot{\mathbf{U}}_1 = -r\mathbf{X} - \frac{L}{2}\mathbf{U}_1 - \frac{5}{2}a\left(V_1 - \frac{4}{9}V_2\right)\mathbf{X}, \qquad (3.16f)$$

$$\tau\dot{\mathbf{U}}_2 = -r\mathbf{X} - \frac{5L}{2}\mathbf{U}_2 - \frac{10}{3}a\left(V_1 - \frac{1}{6}V_2\right)\mathbf{X}. \qquad (3.16g)$$

It is an extension of the standard Lorenz model [42]. The latter is contained in Eqs. (3.16a)–(3.16c) in a form that is slightly modified due to a different scaling and to the realistic no slip boundary conditions in our approximation.

This model can be looked upon as a minimal one for convection in binary liquid mixtures because it contains on the one hand the minimal description of convection in a pure fluid (the Lorenz model) and on the other hand a minimal extension for binary fluids. This extension is minimal since the simple extension [36,37,24,43] of the Lorenz model with only one linear mode $\mathbf{U}$ and one nonlinear mode V leads to TW solutions with linear relations between all pairs of the three quantities v^2 (the square of the phase velocity), w^2 (convective intensity), and the Rayleigh number r. In Ref. [45] it has been shown that such pairwise linear relations result from *any* truncation of the concentration field that is limited to only one linear and one nonlinear mode. Clearly, these pairwise linear relations between v^2, w^2, and r are incompatible with the topology of a backwards Hopf bifurcation followed by a saddle node bifurcation into a branch of stable strongly nonlinear TWs. Thus our incorporation of a second linear mode $\mathbf{U}_2$ and its nonlinear partner mode V_2 can be seen as a first nontrivial step in a (systematic) extension that goes beyond earlier models [36,37,24,43].

Up to now, no few-mode model has described the bifurcation topology of TWs adequately: The problem was not so much the backwards Hopf bifurcation but rather the transition to strongly nonlinear convection, the saddle node, and finally the merging of the TW solution branch with the upper SOC solution branch. This failure of the earlier approximations is due to an insufficient representation of the concentration field: It has not been truncated directly but rather the combination $\zeta = C - \psi T$ with the temperature field has been introduced in order to fulfill the impermeable boundary condition *exactly*. However, when using the combined field ζ, high mode representations in both ζ as well as in T are required as explained in [34]. By enforcing the impermeability of the plates only *in the lateral average* we avoid these difficulties in our truncation (3.12).

As an aside we mention that within another minimal approach Knobloch and Moore [21] have deduced a model for free slip permeable boundary conditions. They aimed at a correct, analytical representation of the primary bifurcation and the involved modes which is possible for idealized boundary conditions. However, their model does not show TWs comparable with those seen in experiments and related simulations.

IV. RESULTS

Here, we elucidate the SOC, TW, and SW solutions of our model.

A. Stationary convection

1. Bifurcation properties of SOC states

In the case of SOC all time derivatives in Eq. (3.16) vanish so that $\mathbf{X}\|\mathbf{Y}\|\mathbf{U}_1\|\mathbf{U}_2$ holds in the complex plane for the amplitudes of the laterally varying modes. Without loss of generality we may therefore choose all modes to be real.

After elimination of the temperature and concentration modes the bifurcation diagram $r_{\text{SOC}}(\mathbf{X}^2)$ can be calculated as

$$r_{\text{SOC}}(\mathbf{X}^2) = \cfrac{1+\mathbf{X}^2}{1+\cfrac{11}{5}a\cfrac{\psi}{L}\cfrac{(1+\mathbf{X}^2)\left[1+\cfrac{25}{99}a\left(\cfrac{\mathbf{X}}{L}\right)^2\right]}{1+\cfrac{185}{36}a\left(\cfrac{\mathbf{X}}{L}\right)^2+\cfrac{625}{648}a^2\left(\cfrac{\mathbf{X}}{L}\right)^4}} \tag{4.1a}$$

$$\underset{\sim}{\overset{\mathbf{X}\gg L}{}} \ \cfrac{1+\mathbf{X}^2}{1+\cfrac{72}{125}\left(\cfrac{L\psi}{\mathbf{X}^2}\right)(1+\mathbf{X}^2)}. \tag{4.1b}$$

The relation (4.1) between r and $\mathbf{X}^2$ can be inverted, e.g., graphically to obtain the standard bifurcation diagram of, say, $\mathbf{X}^2$ vs r. The stationary stability threshold $r_{\text{stat}} = r_{\text{SOC}}(\mathbf{X}=\mathbf{0})$ of the quiescent heat conducting state then is

$$r_{\text{stat}} = \cfrac{1}{1+\cfrac{11}{5}a\cfrac{\psi}{L}} \simeq \cfrac{1}{1+1.527\cfrac{\psi}{L}}. \tag{4.2}$$

It agrees quite well with the result $r_{\text{stat}} \simeq (1+1.538\psi/L)^{-1}$ of Galerkin approximations [43,41] that fulfill the concentration boundary condition exactly.

As a first SOC property we can determine the type of the stationary bifurcation out of the quiescent heat conducting state. For Soret couplings smaller than

$$\psi_{\text{SOC}}^t = -\frac{4}{43a^2}$$

$$\times \cfrac{L^3}{1+\left(\cfrac{557}{774a}\right)L+\left(\cfrac{68}{129}a\right)L^2+\left(\cfrac{32}{215a^2}\right)L^3} \tag{4.3}$$

a subcritical bifurcation is observed: $\partial r/\partial\mathbf{X}^2<0$. The scaling of ψ_{SOC}^t with L^3 agrees with earlier free slip [23] and no slip predictions [25]. For subcritical bifurcations the saddle node is found at

$$r_{\text{SOC}}^s = 1+\frac{12}{5}\sqrt{\frac{2}{5}}\sqrt{-L\psi}+O(L\psi) \tag{4.4a}$$

$$\simeq 1+1.518\sqrt{-L\psi}, \tag{4.4b}$$

in good agreement with the numerically determined result $r_{\text{SOC}}^s \simeq 1+1.636\sqrt{-L\psi}$ [[34] Eq. (4.1)].

Equation (4.1b) shows that for convective amplitudes $\mathbf{X} \gg L$ the Rayleigh number corresponding to a certain amplitude square $\mathbf{X}^2$ deviates from that of the pure fluid $r_{\psi=0} = 1+\mathbf{X}^2$ only by terms $\propto L\psi$. This means that for convective amplitudes $\mathbf{X}^2 \gg L|\psi|$ the bifurcation diagrams of a mixture are the same as for a pure fluid. This equality reflects the fact that strong convective mixing in conjunction with diffusion equilibrates the concentration in the whole fluid with the exception of narrow boundary layers so that it does not in-

fluence the bifurcation behavior any more: The stronger the mixing the smaller the deviation from the pure fluid case.

2. Fields

In order to reconstruct the fields and with them the order parameters such as the Nusselt number N and the concentration variance M, Eq. (2.2), we need the mode amplitudes

$$\mathbf{Y} = \frac{r\mathbf{X}}{1+\mathbf{X}^2}, \tag{4.5a}$$

$$Z = \frac{r\mathbf{X}^2}{1+\mathbf{X}^2}, \tag{4.5b}$$

$$V_1 = -2rF_{\text{SOC}}\left(\frac{\mathbf{X}}{L}\right)^2\left[1+\frac{25}{216}a\left(\frac{\mathbf{X}}{L}\right)^2\right], \tag{4.5c}$$

$$V_2 = -\frac{1}{4}rF_{\text{SOC}}\left(\frac{\mathbf{X}}{L}\right)^2\left[1-\frac{25}{18}a\left(\frac{\mathbf{X}}{L}\right)^2\right], \tag{4.5d}$$

$$\mathbf{U}_1 = -2rF_{\text{SOC}}\left(\frac{\mathbf{X}}{L}\right)\left[1+\frac{5}{12}a\left(\frac{\mathbf{X}}{L}\right)^2\right], \tag{4.5e}$$

$$\mathbf{U}_2 = -\frac{2}{5}rF_{\text{SOC}}\left(\frac{\mathbf{X}}{L}\right)\left[1-\frac{25}{18}a\left(\frac{\mathbf{X}}{L}\right)^2\right] \tag{4.5f}$$

in the SOC fixed points. Here, we have introduced the quantity

$$F_{\text{SOC}} = \left[1+\frac{185}{36}a\left(\frac{\mathbf{X}}{L}\right)^2+\frac{625}{648}a^2\left(\frac{\mathbf{X}}{L}\right)^4\right]^{-1} \tag{4.5g}$$

for notational convenience. The square of M is given by

$$M_{\text{SOC}}^2 = \left[1+3.905\left(\frac{\mathbf{X}}{L}\right)^2+2.224\left(\frac{\mathbf{X}}{L}\right)^4+0.3040\left(\frac{\mathbf{X}}{L}\right)^6\right.$$
$$\left.+0.002\,072\left(\frac{\mathbf{X}}{L}\right)^8\right]$$
$$\times\left[1+3.566\left(\frac{\mathbf{X}}{L}\right)^2+0.4645\left(\frac{\mathbf{X}}{L}\right)^4\right]^{-2} \tag{4.6}$$

and the Nusselt number by

$$N_{\text{SOC}} = 1+\frac{25}{18}\frac{\mathbf{X}^2}{1+\mathbf{X}^2}. \tag{4.7}$$

3. Comparison with numerical results

Using these formulas we can compare the results of the model with ''exact'' ones obtained by a MMG calculation [34]. This is done in Fig. 2 with the bifurcation diagrams of N and M. Since the Nusselt number [Fig. 2(a)] is determined by the well described temperature field the Nusselt number of the model deviates from the ''exact'' one maximally by 1% (at $r=1.6$). The variance of the concentration field M in Fig. 2(b) shows that also the concentration field is approximated reasonably well: the strong mixing in stable SOCs with large velocity amplitudes (upper branch of N and lower
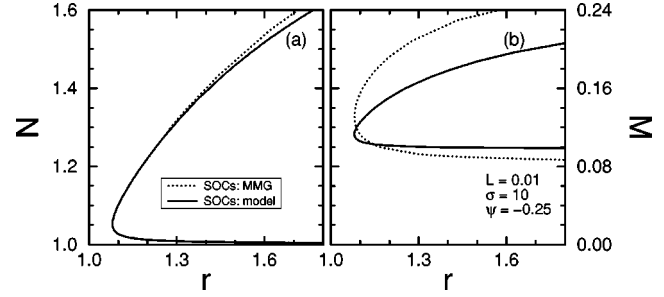
FIG. 2. SOC bifurcation diagrams of Nusselt number N (a) and concentration variance M (b) vs reduced Rayleigh number r. Exact (model) results are shown by dotted (solid) lines.

branch of M) leading to nearly equilibrated concentration distribution and nearly vanishing M is reproduced with a relative error of about 15%. Since with the special mode selection in the concentration field the model was constructed to describe strongly nonlinear convection rather than weakly nonlinear states it is not surprising that M in the unstable SOCs is reproduced only with an accuracy of about 20% at $r=1.6$.

Beyond these global order parameters we may also discuss the spatial variations of the concentration field. In Fig. 3 we compare the SOC concentration field structure obtained from our model with the ''exact'' one from a MMG scheme. To that end we show vertical (right column) and horizontal (left column) profiles. Of course, the model cannot describe the narrow concentration peaks in the lateral direction which are due to the strong boundary layer phenomena caused by the smallness of the ratio $L/w_{\text{max}} = O(0.001)$. Nevertheless, the model predicts that the concentration vanishes nearly all over the convection cell. Also in the vertical profile we see a good agreement when keeping in mind that the combination of only two modes, namely c_{02} and c_{04}, can provide only a very rough approximation to a boundary layer.

The quality of the approximation of the concentration can also be discussed by its zeroth lateral Fourier mode. The model predicts

$$C_0(z) = -\frac{\psi}{5}\left[z-\frac{1}{\pi}\sum_{n=1}^{2}(-1)^{n+1}\frac{\sin n(2\pi z)}{n}\right]+O\left(\frac{L}{\mathbf{X}}\right)^2. \tag{4.8}$$
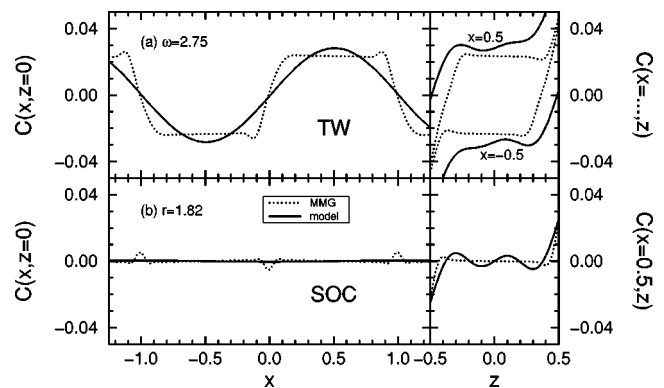
FIG. 3. Lateral (left column) and vertical (right column) concentration profiles of a TW with frequency $\omega=2.75$ (a) and of a SOC (b) at a Rayleigh number of $r=1.82$. The two line types compare model (solid lines) and ''exact'' results (dotted lines). Parameters are $L=0.01$, $\sigma=10$, and $\psi=-0.25$.

In the ''exact'' results [18,34], $C_0(z)$ is nearly zero in the bulk of the fluid outside the boundary layers near the plates. It is interesting to note that an extension of the series in the above expression to $n = \infty$ would yield

$$\frac{1}{\pi} \sum_{n=1}^{\infty} (-1)^{n+1} \frac{\sin n(2\pi z)}{n} = \frac{1}{\pi} \frac{2\pi z}{2} = z \qquad (4.9)$$

for values of $z \in \;]-0.5, 0.5[$ so that the linear term z in the square brackets of Eq. (4.8) is completely canceled. Thus the exact result—$C_0(z) \equiv 0$ in the limit $L \to 0$—is reproduced in an optimal way, namely, by giving the exact results for those modes that the model contains. A significantly improved description is possible only by using many more modes because the contribution from higher modes in Eq. (4.9) decrease only $\propto 1/n$.

To summarize: stationary convection in binary liquid mixtures is described for negative as well as for positive ψ in a semiquantitative way by our model. Beyond topological details of the bifurcation diagrams even the peculiar spatial structures of the concentration field can be explained.

B. Traveling wave convection

1. Bifurcation and scaling properties

For the TW fixed points of the model (3.16) with a frequency ω we have to assume time dependences $\propto e^{i\omega t}$ of the complex modes $\mathbf{X}$, $\mathbf{Y}$, $\mathbf{U}_1$, and $\mathbf{U}_2$ because they are the amplitudes of a lateral variation $\propto e^{-ikx}$. So, positive frequencies correspond for positive wave numbers k to TWs traveling to the right. The zeroth lateral modes Z, V_1, and V_2 are time independent in TWs. We separate the time dependence $e^{i\omega t}$ of the complex amplitude vectors by

$$[\mathbf{X}(t), \mathbf{Y}(t), \mathbf{U}_1(t), \mathbf{U}_2(t)] = [\mathbf{X}, \mathbf{Y}, \mathbf{U}_1, \mathbf{U}_2] e^{i\omega t} \quad (4.10)$$

and use henceforth the same symbols for the time-independent prefactors. Then, by choosing the temporal phase, $\mathbf{X}$ can be taken as real while $\mathbf{Y}, \mathbf{U}_1, \mathbf{U}_2 \in \mathbb{C}$. In addition, $Z, V_1, V_2 \in \mathbb{R}$. Inserting these solution *Ansätze* into Eq. (3.16) yields in order $O(L^0)$ the relations

$$-\frac{1}{\psi} = \frac{3}{2} a \frac{\widetilde{\sigma}}{\widetilde{\sigma}+1} \frac{1+\Omega^2+\mathbf{X}^2}{\Omega^2}$$

$$\times \frac{1 + \dfrac{175}{108} a \left(\dfrac{\mathbf{X}}{\Omega}\right)^2}{1 + \dfrac{1025}{144} a \left(\dfrac{\mathbf{X}}{\Omega}\right)^2 + \dfrac{15\,625}{10\,368} a^2 \left(\dfrac{\mathbf{X}}{\Omega}\right)^4},$$

$$(4.11a)$$

$$r_{\mathrm{TW}} = 1 + \Omega^2 + \mathbf{X}^2 \qquad (4.11b)$$

between frequency ω, amplitude $\mathbf{X}$, and control parameter r_{TW} of the TW solution. Here,

$$\Omega = \omega \tau \qquad (4.11c)$$

has been introduced with $\tau = 1/2\pi^2$, Eq. (3.14e), being the intrinsic time scale of the model (3.16).

Neglecting terms $O(L)$ in Eq. (4.11) causes the TW to merge at $\omega = 0$ with the SOC solution branch of the pure fluid instead of with the SOC solution (4.1) of the mixture. Canceling the terms of $O(L^2)$ is allowed for all states with $L \ll \Omega$ or $L \ll \mathbf{X}$. This condition is fulfilled for all separation ratios away from the codimension-2 (CT) point where Hopf bifurcation *and* SOC-TW merging fall together and none of the relations $L \ll \Omega$ or $L \ll \mathbf{X}$ can be fulfilled. The TW fixed points of our model can be calculated analytically without limiting to the order $O(L^0)$. Since the formulas are lengthy they are not presented here. But they have been used for the calculation of the phase diagram in Fig. 9 including the CT point.

From Eq. (4.11a) one observes first of all that TWs exist only for negative Soret couplings $\psi < 0$. This is in line with the absence of TWs for $\psi > 0$ in numerical simulations—TWs for $\psi > 0$ seen in the model of Ref. [24] result from low-order truncation. Relation (4.11b) allows us to determine the frequency Ω of a TW with a given velocity amplitude $\mathbf{X}$:

$$r_{\mathrm{TW}}(\mathbf{X}^2) = 1 + \mathbf{X}^2 + \Omega^2(\mathbf{X}^2)$$

$$= r_{\psi=0}(\mathbf{X}^2) + \Omega^2(\mathbf{X}^2) \qquad (4.12a)$$

or

$$\frac{\omega^2(\mathbf{X}^2)}{\omega_H^2} = \frac{r_{\mathrm{TW}}(\mathbf{X}^2) - r_{\psi=0}(\mathbf{X}^2)}{r_{\mathrm{osc}} - 1}. \qquad (4.12b)$$

Thus the model predicts that the square of the frequency Ω of a TW state with a velocity amplitude $\mathbf{X}$ is the distance in the control parameter r between the TW under consideration and the state of the pure fluid with the same velocity amplitude. Hence the TW frequency is a direct measure of the distance of the system from the pure fluid, i.e., the influence of the concentration.

Another equivalent interpretation of Eq. (4.11b) is that for a given fixed r the squared frequency of a TW with velocity amplitude $\mathbf{X}_{\mathrm{TW}}$,

$$\Omega^2 = \mathbf{X}_{\psi=0}^2 - \mathbf{X}_{\mathrm{TW}}^2, \qquad (4.13)$$

is given by the difference between the pure fluid flow intensity, $\mathbf{X}_{\psi=0}^2 = r - 1$, and the flow intensity $\mathbf{X}_{\mathrm{TW}}^2$ of the TW in question. Thus Ω^2 measures also the ''vertical'' distance in the bifurcation diagrams of $\mathbf{X}^2$ vs r between the $\psi = 0$ pure fluid SOC solution and the TW solution in the mixture.

Equation (4.12a) has an explicit dependence on the Soret coupling strength ψ since Ω varies between 0 and the scaled Hopf frequency Ω_H. This ψ dependence is canceled by scaling Eq. (4.12a) with the Hopf frequency so that the left hand side of Eq. (4.12b) varies for all ψ between 0 and 1. Thus Eq. (4.12b) is a universal scaling relation for TW frequencies resulting from our model for small L. In Fig. 4 this prediction of the model is compared with numerical results for $\psi \in [-0.65, -0.25]$ obtained by a finite difference scheme and a MMG scheme [20]. For all these Soret couplings the scaling relation is confirmed by the numerical results. Only in the case of small frequencies are deviations observed. They are due to the fact that TWs with small frequencies do not
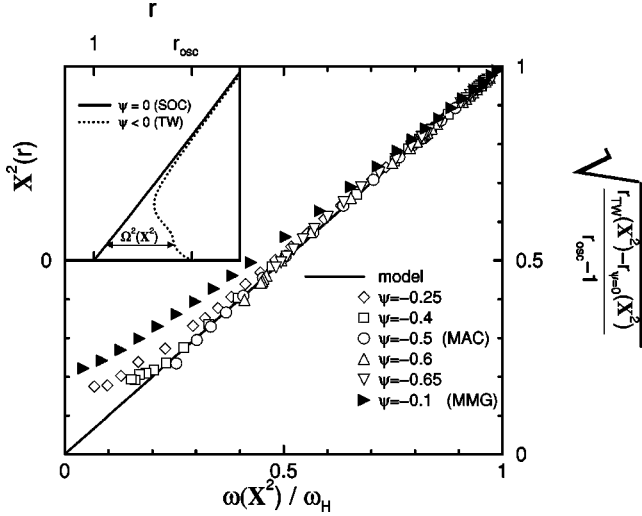
FIG. 4. Universal scaling relation connecting TW convective velocity amplitude $\mathbf{X} \propto w_{max}$ with its frequency ω. The model prediction (4.12b) is the identity (solid line). Numerical, finite difference (MAC) data are shown by open symbols for $\psi \in [-0.25, -0.65]$ and MMG data by filled symbols ($\psi = -0.1$). The symbols cover in each case the whole bifurcation branch, i.e., stable as well as unstable TW states. The inset serves as a schematic explanation of the scaling relation. L and σ were fixed to values of 0.01 and 10, respectively. But the scaling relation should not depend on them as long as $\sigma \gtrsim 1$ and $L \ll 1$.

approach the SOC states of the pure fluid as implied by Eq. (4.11b) but rather the SOC states of the mixture. These two stationary states differ in the Rayleigh number r by $O(L)$ according to Eq. (4.1b) so that deviations of the order $O(\sqrt{L}) \simeq 0.1$ can be expected on the ordinate of Fig. 4. This deviation from the scaling relation becomes more obvious for weaker Soret couplings like, e.g., $\psi = -0.1$, as shown by the filled triangles. These states have been computed by a MMG scheme [34]. For small Soret couplings the merging point of the SOC and TW branches is in a regime of small velocity amplitudes, i.e., in that part of the bifurcation diagram where the differences between SOC states of pure and binary mixed fluids become more and more evident.

It should be noticed that the scaling relation holds for stable as well as for unstable TWs. Furthermore, it is independent of the bifurcation topology, i.e., it applies to the form shown in the inset of Fig. 4, i.e., for $\psi \gtrsim -0.4$ as well as to a topology with a bistability of slow and fast TWs ($\psi \lesssim -0.4$) [20].

Bifurcation properties are best discussed by introducing the ratio

$$\chi = \frac{w_{max}}{v} = \frac{5\pi}{8} \frac{|\mathbf{X}|}{\Omega} \qquad (4.14)$$

of convective and phase velocity of the TW state. Then, the Rayleigh number $r_{TW}(\chi^2)$ of a TW with a velocity ratio χ can be written in order $O(L^0)$ as

$$r_{TW}(\chi^2) = \frac{1}{1 + \dfrac{27\pi^2}{256} \psi \dfrac{\widetilde{\sigma}}{1+\widetilde{\sigma}} \dfrac{\left[1 + \left(\dfrac{64}{25\pi^2}\right)\chi^2\right]\left(1 + \dfrac{7}{24}\chi^2\right)}{1 + \dfrac{41}{32}\chi^2 + \dfrac{25}{512}\chi^4}} . \qquad (4.15)$$

The oscillatory stability threshold of the basic state follows for $\chi = 0$ as

$$r_{osc} = r_{TW}(0) = \frac{1}{1 + \left(\dfrac{27\pi^2}{256}\right)\left(\dfrac{\widetilde{\sigma}}{(1+\widetilde{\sigma})}\right)\psi} \qquad (4.16a)$$

and Eq. (4.11b) yields the Hopf frequency

$$\omega_H^2 = \frac{-\left(\dfrac{27\pi^6}{64}\right)\psi}{\dfrac{(1+\widetilde{\sigma})}{\widetilde{\sigma}} + \left(\dfrac{27\pi^2}{256}\right)\psi} \simeq \frac{-405.6\psi}{\dfrac{(1+\widetilde{\sigma})}{\widetilde{\sigma}} + 1.041\psi} . \qquad (4.16b)$$

The calculation of the CT point requires the consideration of the Lewis number dependence. If this is done one obtains

$$\psi^{CT} = -\frac{1600}{459\pi^2} \frac{\widetilde{\sigma}+1}{\widetilde{\sigma} + \dfrac{55}{102}L} L^2 \qquad (4.17)$$

as the separation ratio at the CT point for given Lewis and Prandtl number and fixed wave number $k = \pi$. In ethanol-water mixtures with $L = 0.01$ and $\sigma = 10$, this yields $\psi^{CT} = -3.714 \times 10^{-5}$ which is in very good agreement with the numerically [25] determined value of -3.526×10^{-5}.

The other limit in χ, namely, $\chi \to \infty$ or $\omega \to 0$, gives the Rayleigh number of the SOC-TW transition:

$$r^* = \lim_{\chi \to \infty} r_{TW}(\chi^2) = \frac{1}{1 + \dfrac{1008}{625}\left(\dfrac{\widetilde{\sigma}}{(1+\widetilde{\sigma})}\right)\psi} . \qquad (4.18)$$

However, one should keep in mind that the SOC-TW transition at r^* with the transfer of stability from a SOC to a TW when reducing r is related to an instability of the SOC concentration boundary layer [19]. These boundary layers are caused by the smallness of the Lewis number L, a limit which is not systematically incorporated in the model under consideration. The model's main objective is a description of strongly nonlinear TW convection which has for finite TW frequencies a definite limit for small L. Thus one should not expect a correct reproduction of the Lewis number dependence of the SOC-TW transition from a model with modes that do not resolve the boundary layer structure in detail. However, the dependence on the two other fluid parameters, namely, separation ratio ψ and Prandtl number σ, is given in a qualitatively correct way: strong increase of r^* with stronger negative Soret coupling and saturation with increasing σ

as can be seen by comparing the formula (4.18) with the numerical results in Figs. 9(b) and 15(b) of Ref. [18]. The SOC-TW transition points which have been plotted therein are also affected with a certain error bar since the spatial resolution of the numerical method used was not fine enough to capture the whole boundary layer phenomena. However, their qualitative fluid parameter dependence has to be regarded as correct.

The analytical form (4.15) for the TW bifurcation diagram allows a simple determination of the TW saddle node bifurcation, namely, as the minimum of $r_{\rm TW}(\chi^2)$. It is given by

$$r_{\rm TW}^s \simeq r_{\rm TW}(2.8687) \simeq \frac{1}{1+0.6567\left(\dfrac{\widetilde{\sigma}}{(1+\widetilde{\sigma})}\right)\psi}. \quad (4.19)$$

2. Fields

The calculation of Nusselt number N, concentration variance M, and concentration contrast between the two plates requires the computation of the temperature and concentration field in the TW fixed points. Their mode amplitudes in the TW fixed points can be expressed by

$$V_1 = -\frac{32}{5\pi^2}\chi^2 r F_{\rm TW}\left(1+\frac{5}{192}\chi^2\right),$$

$$V_2 = -\frac{4}{\pi^2}\chi^2 r F_{\rm TW}\left(1-\frac{1}{16}\chi^2\right),$$

$$\mathbf{U}_1 = -\frac{\mathbf{X}}{\Omega}\left(\frac{L}{2\Omega}-i\right)\tau F_{\rm TW}\left(1+\frac{15}{32}\chi^2\right), \quad (4.20a)$$

$$\mathbf{U}_2 = -\frac{\mathbf{X}}{\Omega}\left(\frac{5L}{2\Omega}-i\right)\tau F_{\rm TW}\left(1-\frac{1}{16}\chi^2\right),$$

$$\mathbf{Y} = \mathbf{X}(1-i\Omega),$$

$$Z = \mathbf{X}^2,$$

where we have introduced the quantity

$$F_{\rm TW} = \left(1+\frac{41}{32}\chi^2+\frac{25}{512}\chi^4\right)^{-1}. \quad (4.20b)$$

In Eq. (4.20a) all quantities except the real parts of $\mathbf{U}_1$ and $\mathbf{U}_2$ are evaluated in order L^0 with $\mathbf{X}$ and Ω taken from Eq. (4.11).

3. Small amplitude expansions

Before discussing the order parameters themselves we should like to show that they *cannot* be expanded as power series in the distance

$$\epsilon = \frac{r_{\rm TW}(\chi^2)-r_{\rm osc}}{r_{\rm osc}} \quad (4.21)$$

from the onset of convection up to values where strongly nonlinear TW convection is observed. To see this, let us rewrite Eq. (4.21) by using Eq. (4.15) to display the relation between ϵ and χ^2 explicitly,

$$\epsilon = \frac{a_1\chi^2(1+a_2\chi^2)}{1+b_1\chi^2+b_2\chi^4} = \frac{a_1\chi^2(1+a_2\chi^2)}{(1-\chi^2/b_1')(1-\chi^2/b_2')}. \quad (4.22)$$

Here, $a_{1,2}$, $b_{1,2}$, and $b_{1,2}'$ are amplitude-independent real numbers. Note, in particular, that the functional relation between control parameter ϵ and reduced order parameter $\chi = w_{\rm max}/v$ is given by a rational function. A similar relation has also been found from a fit to MMG and finite difference numerical results [20]. The radius of convergence of a small amplitude expansion of Eq. (4.22) in powers of χ^2 is given by

$$\chi_c^2 = \min_{i=1,2}|b_i'|.$$

This quantity depends on ψ and σ so that for all negative values of ψ [TWs are observed only for $\psi<0$ according to Eq. (4.11a)]

$$\chi_c^2 \leq \frac{328}{25}\left(1-\sqrt{\frac{1481}{1681}}\right) \simeq 0.8052,$$

which is the absolute value of that node of $F_{\rm TW}^{-1}(\chi^2)$, Eq. (4.20b), with the smallest absolute value. Then, the radius of convergence is calculated in the variable $w_{\rm max}/v$ as

$$\left(\frac{w_{\rm max}}{v}\right)_c = \chi_c \simeq 0.8973, \quad (4.23)$$

i.e., near that point in the bifurcation diagram which has been identified in [20] as the transition between weakly and strongly nonlinear convection. This point, namely, $w_{\rm max}\simeq v$, where areas of closed streamlines first occur, has also been identified as the radius of convergence for a small amplitude power series expansion of different order parameters (see Ref. [20]).

Thus our model supports the notion that experimentally observed TW convection in binary liquid mixtures *cannot* be described by weakly nonlinear models as, e.g., complex Ginzburg-Landau (GL) amplitude equations including various *ad hoc* quintic extensions that have been proposed. Being used out of their validity range they cannot be trusted to reproduce, e.g., the relations between frequency ω, mixing M, flow intensity $w_{\rm max}^2$ or Nusselt number N, and the thermal driving r. Typically already the simpler relation between $w_{\rm max}^2$ or N and r is wrong on the upper TW branch—not to mention the more sensitive relations between ω, M, and r. Also results for LTWs based on this approach [28] have to be questioned: The spatiotemporal field properties under the envelope being closely related to those in extended TWs are not captured properly. The main drawback of these GL approaches is the insufficient representation of the role of the concentration field in these strongly nonlinear states.

A first step towards a better incorporation of the concentration field into the GL framework was the introduction of a
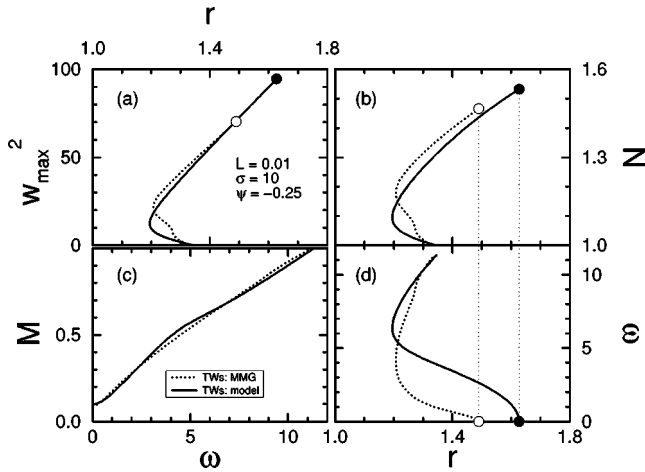
FIG. 5. TW bifurcation diagrams of the square of the convective velocity amplitude w_{max}^2 (a), the Nusselt number N (b), and the frequency ω (d), each vs r. In (c) the reduced concentration variance M is plotted vs frequency.

long wavelength concentration mode with characteristic time scale $\propto L$ by Riecke [29]. The approximation is that L is of the same order as the distance from onset which, however, does not apply to all experimental LTWs. Additionally, those parameters (h_1 and h_3 in Ref. [29]) that could immediately lead in extended TW states without large-scale lateral variation to a finite mean concentration mode (possibly at the expense of stabilizing terms of unphysical fifth order) have been dropped in the LTW calculations [29]. While this approach in its present form does not seem to generate the spatiotemporal field structure of TWs under the LTW envelope it is a promising step forward. Incorporation of impermeable boundary conditions and separation of diffusive (L) and critical (ϵ) time scales and thus the incorporation of an additional concentration mode seems necessary to guarantee the aforementioned relations between ω, M, N, and r.

4. Comparison with numerical results

For a quantitative comparison with numerical MMG results [34] we present in Fig. 5 bifurcation diagrams of the square of convective amplitude (a), the Nusselt number (b), the TW frequency (d), and the concentration variance as a function of the frequency (c). They show that all characteristic features of the TW bifurcation scenario are captured by the model: subcritical Hopf bifurcation, saddle node bifurcation, stable upper branch of strongly nonlinear TWs, merging of TWs and SOCs at $\omega = 0$ in the strongly nonlinear regime, and drastic reduction of the concentration contrast with decreasing frequency. As an aside we mention that a model using the same number of modes, but numerically determined ones, is similarly successful [39]. This has to be contrasted with *earlier analytical* few-mode approximations for TWs in binary mixtures which reproduced only the backwards Hopf bifurcation.

The linear and weakly nonlinear bifurcation properties, i.e., the onset of convection and the initial slope, are modeled by our approximation with high accuracy. The characteristic bump in the ''exact'' bifurcation diagrams of Fig. 5(a), 5(b),

and 5(d) that occurs at the transition $\chi \simeq 1$ from weakly to strongly nonlinear convection is not reproduced by our model. The absence of this fine structure in the bifurcation diagram of our model is due to neglecting Fourier modes higher than the first lateral one in the concentration. We have explicitly checked this by determining the bifurcation diagrams for fields restricted to their zeroth and first lateral Fourier modes but with full vertical resolution. This is also clear from studying the changes in the concentration at that point: Starting at the onset, only harmonic lateral variation is observed up to a velocity ratio $\chi = w_{max}/v \simeq 1$. For larger χ, the harmonic profile gets more and more deformed by the occurrence of plateaus ([20], Fig. 2). They reflect homogenized concentration distributions in the regions of closed streamlines. The description of this equilibration requires higher lateral Fourier modes.

The next characteristic point is the position of the TW saddle node bifurcation: As a consequence of the dropping of higher lateral Fourier modes and the above discussed implications, the saddle lies at too high frequencies or too low amplitudes, i.e., in a too weakly nonlinear part of the bifurcation diagram. On the upper (lower) branch of the N vs r (ω vs r) curve the TW frequeny of our model has too high values [Fig. 5(d)] and the zero frequency TW end point at r^* lies above the ''exact'' one. This is caused by the fact that slow TWs are boundary layer dominated. This feature is not fully reflected in our model.

Since the concentration changes significantly with frequency it is appropriate to discuss the relation between concentration variance M and TW frequency ω [Fig. 5(c)] rather than the relation between M and r, thereby eliminating partly the errors in our ω vs r curve of Fig. 5(d). The prediction of the model for $M(\omega)$ agrees very well with the ''exact'' curve in Fig. 5(c). This is once more a hint that the concentration field is globally treated in an adequate manner. Additionally, the relation between M and ω is a second universal, ψ-independent, scaling relation when scaling the frequency with its value at the Hopf bifurcation. This is done in Fig. 5(b) of Ref. [20] with numerical data.

The spatial variation of the concentration field in a TW is shown in Fig. 3(a). To measure the quality of the model we compare its results with numerically obtained fields. As described above, it is convenient to select for this procedure two TWs with the same frequency but different Rayleigh numbers. The ''effective'' value of the harmonic lateral profile [left part of Fig. 3(a)] in the model corresponds well with the ''exact'' plateaulike concentration distribution. In the vertical profile [right part of Fig. 3(a)], even a slight building up of a plateau can be observed. Its mean height is approximated by the height of the lateral profile explaining the differences in the heights of the vertical plateaus. The strong variation of the model concentration along the plates is an artifact of only approximately fulfilling the impermeability of the plates.

In the actual TW states, the concentration at the plates is nearly constant so that also the contrast between them is nearly constant. Thus an appropriate quantity to compare is the laterally averaged concentration contrast at the two plates. Our model predicts that
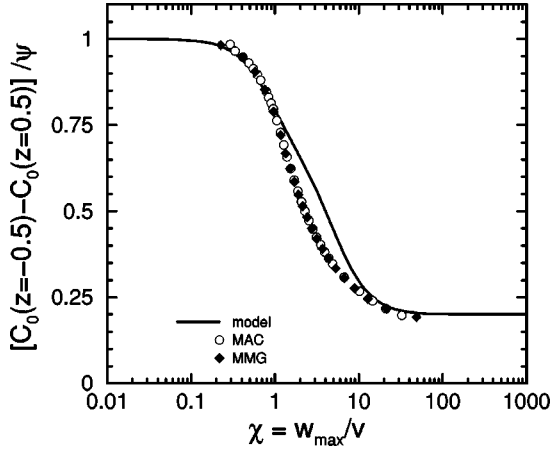
FIG. 6. Concentration contrast in a TW state between the plates as a function of the velocity ratio $\chi = w_{max}/v$ from the model (solid line) and from numerical computations (finite differences: open circles; many-mode Galerkin: filled lozenges). Parameters are $L = 0.01$, $\sigma = 10$, and $\psi = -0.25$.

$$C_0\left(z = \frac{1}{2}\right) - C_0\left(z = -\frac{1}{2}\right) = 2C_0\left(z = \frac{1}{2}\right)$$

$$= -\psi\left(1 - \frac{7}{16}\chi^2 \frac{1 + \frac{5}{56}\chi^2}{1 + \frac{41}{32}\chi^2 + \frac{25}{512}\chi^4}\right) \quad (4.24)$$

$$\xrightarrow{\omega \to 0} -\frac{\psi}{5}$$

depends only on the velocity ratio w_{max}/v. This relation is checked in Fig. 6 by comparing the model prediction with numerical finite differences and MMG results. The two limits, namely, the basic state with $w_{max} \to 0$ and the stationary state $v \to 0$ ($\chi \to \infty$) are reproduced very well by our approximation. The transition between them takes place for $\chi \in [1,10]$.

C. Standing wave convection

Besides SOC and TW convection there exists a third type of convection that bifurcates out of the ground state: It is standing wave convection occurring at a Hopf bifurcation simultaneously with TW convection. As long as linear states are considered SWs are just a linear superposition of a right and left traveling wave. The selection of the nonlinear pattern leading to either a TW or SW is governed by a general principle [46]: stable solutions exist directly at a Hopf bifurcation only if both SW *and* TW bifurcate supercritically. Then, the pattern with the largest initial slope of the amplitude is selected. Using this principle and the numerically obtained initial slopes of [25] it can be inferred that in all liquid mixtures TWs are stable when bifurcating supercritically, i.e., for ψ larger than the tricritical value $\psi_{TW}^t \propto -L^2$. Thus SWs cannot be observed directly in experiments with liquid mixtures. Their investigation requires stabilizing that unstable fixed point and possibly destabilizing the stationary fixed point having the same symmetries. Nevertheless, SWs
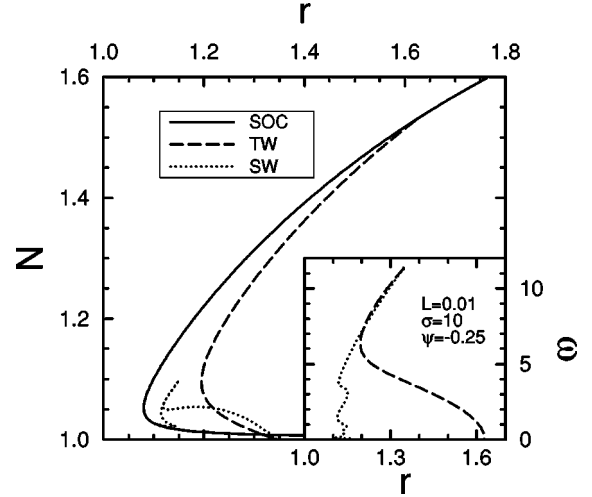
FIG. 7. Complete bifurcation diagram of the Nusselt number (time averaged for SWs) of all types of convection connected with the ground by a primary bifurcation: stationary convection (SOC), traveling (TW), and standing (SW) waves. The inset shows the frequency bifurcation diagrams of TWs and SWs.

represent a generic convection pattern in binary fluid mixtures. They occur, in particular, as transients in the evolution of a strongly nonlinear TW out of the unstable, supercritically heated ground state.

Up to now, only weakly nonlinear properties as the initial slope of SWs have been discussed for binary fluid mixtures with experimentally realistic, i.e., impermeable boundary conditions. Since our model (3.16) has described both SOCs and TWs in an adequate way we think it is worthwhile to equally investigate the bifurcation properties and time dependence of SWs in its framework. The computation of the SW fixed points using the full field equations is a problem which has not been solved so far.

1. Solution procedure

In SWs the phases of the complex modes $\mathbf{X}$, $\mathbf{Y}$, $\mathbf{U}_1$, and $\mathbf{U}_2$ are time independent so that the time derivative is parallel to the mode itself, e.g., $\mathbf{X} \| \dot{\mathbf{X}}$. Via the model (3.16) this leads to $\mathbf{X} \| \mathbf{Y} \| \mathbf{U}_1 \| \mathbf{U}_2$, i.e., all modes may be chosen real without restriction of generality.

In the linear modes $\mathbf{X}$, $\mathbf{Y}$, $\mathbf{U}_1$, and $\mathbf{U}_2$ only odd multiples of the basic frequency ω of the SW occur whereas in the nonlinear modes Z, V_1, and V_2 only even multiples exist. This allows us to expand the time dependence of the mode amplitudes in the following way:

$$[\mathbf{X}(t), \mathbf{Y}(t), \mathbf{U}_1(t), \mathbf{U}_2(t)]$$

$$= \sum_{n=1,3,5,\ldots} [\mathbf{X}^{(n)}, \mathbf{Y}^{(n)}, \mathbf{U}_1^{(n)}, \mathbf{U}_2^{(n)}]e^{in\omega t} + \text{c.c.}, \quad (4.25a)$$

$$[Z(t), V_1(t), V_2(t)] = \sum_{n=0,2,4,\ldots} [Z^{(n)}, V_1^{(n)}, V_2^{(n)}]e^{in\omega t} + \text{c.c.} \quad (4.25b)$$

These series can be inserted in the model (3.16), the mode amplitude $\mathbf{X}^{(1)}$ can be chosen real by the arbitrariness of a common phase in time, and the resulting nonlinear system of
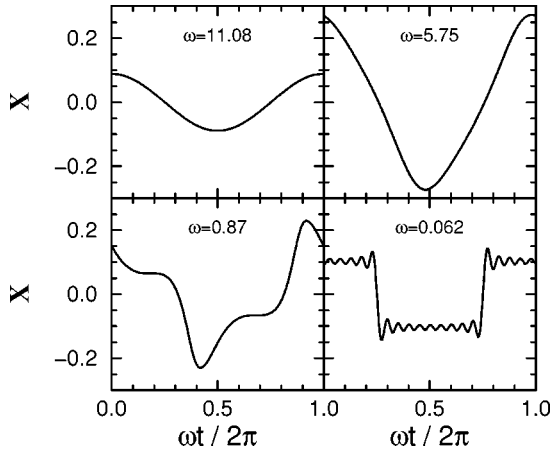
FIG. 8. Time dependence of the velocity field amplitude **X** over one oscillation period in SWs with four different frequencies. Parameters are $L=0.01$, $\sigma=10$, and $\psi=-0.25$.

algebraic equations can be solved in the unknown variables $\{\omega, \mathbf{X}^{(1)}, \text{Re } \mathbf{X}^{(3)}, \text{Im } \mathbf{X}^{(3)}, \ldots\}$.

2. Bifurcation diagram and temporal behavior

In Fig. 7 a bifurcation diagram of the time averaged Nusselt number in SWs (dotted line) is given for the standard ethanol-water fluid parameters together with the already discussed diagrams for SOCs (solid line) and TWs (dashed line). The inset shows the frequency of SW and TW. At the oscillatory onset of convection ($r_{osc}\simeq1.345$) both TWs and SWs bifurcate subcritically as has been predicted by [25]. With decreasing frequency a weak maximum in the time averaged Nusselt number of the SWs is observed ($r\simeq1.19$) before a saddle node occurs at $r\simeq1.12$. Then, it increases with further decreasing frequency up to an absolute maximum of about 1.1 before approaching the SOC branch. The SW branch has to be connected with the SOC branch since a SW with frequency 0 is a SOC. The exact merging point of SWs and SOCs cannot be determined by means of Eq. (4.25) since with decreasing frequency the time dependence of the modes gets more and more anharmonic so that in the Fourier *Ansatz* (4.25) more and more modes have to be included. The evolution of this anharmonicity with decreasing frequency is indicated in Fig. 8 where the time dependence of the velocity field mode **X** within one period of oscillation is plotted.

For the computation of the SWs shown in Fig. 7 and Fig. 8 temporal Fourier modes up to 10ω have been used and compared with states calculated with modes up to 20ω. Between ω_H and $\omega=0.4$ the results of both time resolutions agree in Nusselt and Rayleigh number better than 1% for fixed frequency. However, states with $\omega<0.4$ shown in Fig. 7 and Fig. 8 may be erroneous.

D. Phase diagram

The dependence of the bifurcation topology of SOCs and TWs on the separation ratio is summarized in the phase diagram of Fig. 9 which can be compared directly with the "exact" results described in Fig. 7 of Ref. [34]. The characteristic points of the SOC bifurcation diagrams, namely, the stationary onset r_{stat} and the saddle node r_{SOC}^s, agree very
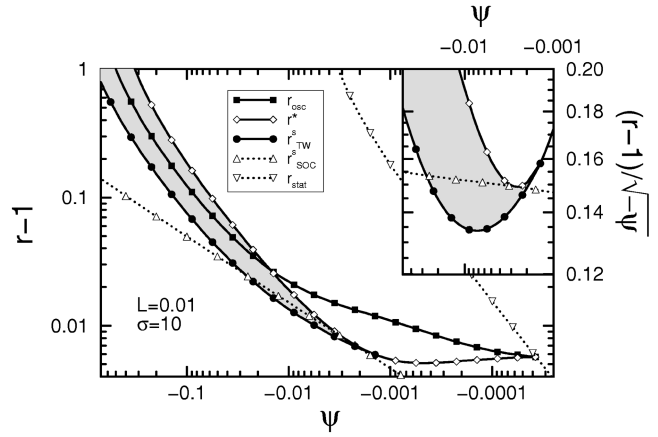
FIG. 9. Phase diagram in mixtures with $L=0.01$ and $\sigma=10$ in a double logarithmical plot $r-1$ vs ψ. SOC properties are shown by dotted lines (saddle node r_{SOC}^s: open triangles up; bifurcation r_{stat}: open triangles down). Solid lines correspond to TWs (Hopf bifurcation r_{osc}: filled squares; SOC-TW transition r^*: open lozenges; saddle node r_{TW}^s: filled circles). Stable TWs exist within the shaded area.

well with the "exact" results. The same holds without restriction for the oscillatory onset of convection r_{osc} and the TW saddle node bifurcation r_{TW}^s. The ψ dependence of the SOC-TW transition point r^*, i.e., the strong increase with increasing the negative coupling strength, is only reproduced qualitatively: $r^*(\psi)$ runs too flat in the interval $[-0.3, -0.01]$ so that the point where $r^*\equiv r_{osc}$ is given as $\psi\simeq -0.014$ instead of -0.14. This is due to the neglect of the influence of boundary layers in the concentration field. The same is true for the merging of r^* with the TW saddle node, i.e., that separation ratio beyond which no stable upper TW branch can be observed: $\psi\simeq-0.001$ instead of -0.008. Nevertheless, the model predicts a ψ interval where the TW saddle node can be seen below the SOC saddle node, as it has been discussed in the framework of the "exact" results in Fig. 5(d) of Ref. [34]. Furthermore, the tricritical SOC-TW transition [[34], Fig. 5(e)] at which the TW branch merges vertically with the SOC branch, is predicted to take place on the unstable SOC branch, too. For more negative ψ a TW saddle appears. Then, stabilization of TWs at that saddle *and* subsequent destabilization, probably towards modulated TWs, occurs before the now unstable TWs end on the unstable lower SOC branch ([34], Fig. 6).

V. CONCLUSION

We have investigated roll-like 2D convection in binary liquid mixtures with negative Soret coupling. Then, three types of extended convective states occur which are connected via a primary bifurcation to the quiescent heat conducting state: stationary convection (SOC), traveling waves (TW), and standing waves (SW). One objective of our paper was to derive a model describing the combined SOC-TW bifurcation topology and the characteristic spatiotemporal behavior of the concentration seen in numerical simulations and experiments. The most important TW bifurcation features are (i) a backwards Hopf bifurcation, (ii) a saddle node giving rise to stable TWs, and (iii) the merging of the TW solution branch with the SOC branch. Along the TW branch,

(iv) both the phase velocity and the variance of the concentration field decrease monotonically in the same way.

Model. To derive such a model we started with an approximation for velocity and temperature fields similar to that in the standard Lorenz model [42]. We used, however, a more realistic improved version with a no slip velocity field. To select and motivate an appropriate representation of the concentration field we relied on a systematic analysis of the concentration balance equations: the structure of the field components occurring in a symmetry decomposition was investigated [39], a separation into lateral mean fields and deviations thereof was used, and the effect of the Soret coupling in the bulk of the fluid layer and at the plates was quantitatively assessed for liquid mixture parameters [34]. The concentration field truncation derived from these investigations consists of two linear and two nonlinear modes. The resulting Galerkin model can be looked upon as minimal for the description of convection in binary liquid mixtures since it contains the Lorenz model, i.e., the simplest truncation for the pure fluid, and a minimal extension for mixtures. Previous extensions [36,37,24,43] of the Lorenz model were too simple and therefore failed in reproducing strongly nonlinear properties such as, e.g., the TW saddle node. The present model is the first analytically manageable approximation showing the above stated four characteristic properties (i)–(iv).

Stationary convection. Good agreement in the properties of the SOC branch was found: stability threshold, fluid parameters at the tricritical bifurcation, and position of the saddle node bifurcation. Furthermore, the approach of the SOC branch of a binary mixture to that of a pure fluid could be discussed in the limit of large convective amplitudes. Even the spatial variations of the concentration field which is boundary layer dominated in SOCs are reproduced in a way allowing good quantitative agreement in the concentration variance. This holds for both negative and positive ψ.

Traveling waves. The main results have to be seen in the description of TWs. Here, the model shows that TWs occur only for negative Soret couplings in agreement with all numerical simulations and experiments. It predicts that the TW frequency is a direct measure for the ''distance'' of the system from the pure fluid, i.e., for the influence of the concentration field. The ''distance'' can directly be read off the bifurcation diagrams of flow intensity versus Rayleigh number in two equivalent geometric ways. This insight yielded a universal scaling relation between phase velocity, convective velocity, and degree of mixing of a TW which was confirmed in an impressive manner by different numerical methods analyzing the full field equations. The derived scaling relation holds for all TW states, stable or unstable independent of the bifurcation topology [20].

Linear convective properties are reproduced by the model with high accuracy: oscillatory stability threshold, Hopf frequency, and CT point. The same holds for the Rayleigh number at the saddle node bifurcation. Our model shows also a SOC-TW transition to SOCs at the upper stationary stable branch and its dependence on the separation ratio and Prandtl number is qualitatively correct. However, its Lewis number dependence is unphysical since the concentration boundary layers which are responsible for the SOC-TW transition [19] are represented in the model only in an incomplete way. Otherwise, the spatial structure of the concentration field in TWs—frequency dependence of the concentration contrast between the two plates and building up of plateaus (in the vertical direction)—is modeled in a quantitatively correct way by our truncation.

The model allows us to pinpoint the breakdown of an expansion of the TW solution as a power series in the distance from the onset of convection up to values where stable, strongly nonlinear TWs are observed in experiments. The related radius of convergence of the model is close to the numerically determined one [20] marking the transition from weakly to strongly nonlinear states [20]. Hence complex Ginzburg-Landau equations should not be expected to yield reliable quantitative results for localized and extended TW states.

The results of the stationary and traveling states are brought together in a phase diagram whose good agreement with numerical simulations [34] can directly be inferred. Only in the SOC-TW transition are remarkable deviations observed.

Standing waves. Our model gives insights into nonlinear SW solutions in binary mixtures. It confirms earlier weakly nonlinear results [46,25] like the initial slope. In addition, it becomes possible to follow the SW branch, which is everywhere unstable, up to regions with strongly nonlinear oscillating amplitudes. A numerical determination of the unstable SW solution of the full field equations is still lacking and an observation of these states, say, by a control process is an experimental challenge.

[1] M. C. Cross and P. C. Hohenberg, Rev. Mod. Phys. **65**, 851 (1993).

[2] R. W. Walden, P. Kolodner, A. Passner, and C. M. Surko, Phys. Rev. Lett. **55**, 496 (1985).

[3] D. R. Ohlsen, S. Y. Yamamoto, C. M. Surko, and P. Kolodner, Phys. Rev. Lett. **65**, 1431 (1990).

[4] H. Touiri, J. K. Platten, and G. Chavepeyer, Eur. J. Mech. B Fluids **15**, 241 (1996).

[5] G. Ahlers and I. Rehberg, Phys. Rev. Lett. **56**, 1373 (1986).

[6] J. L. Liu and G. Ahlers, Phys. Rev. Lett. **77**, 3126 (1996); Phys. Rev. E **55**, 6950 (1997).

[7] H. Gao and R. P. Behringer, Phys. Rev. A **34**, 697 (1986).

[8] E. Moses and V. Steinberg, Phys. Rev. Lett. **60**, 2030 (1988).

[9] K. D. Eaton, D. R. Ohlsen, S. Y. Yamamoto, C. M. Surko, W. Barten, M. Lücke, M. Kamps, and P. Kolodner, Phys. Rev. A **43**, 7105 (1991).

[10] G. Zimmermann and U. Müller, Int. J. Heat Mass Transf. **35**, 2245 (1992).

[11] B. L. Winkler and P. Kolodner, J. Fluid Mech. **240**, 31 (1992).

[12] A. La Porta, K. D. Eaton, and C. M. Surko, Phys. Rev. E **53**, 570 (1996).

[13] L. D. Landau and E. M. Lifshitz, *Hydrodynamik* (Akademie-Verlag, Berlin, 1966).

[14] J. K. Platten and J. C. Legros, *Convection in Liquids* (Springer-Verlag, Berlin, 1984).

[15] W. Barten, M. Lücke, W. Hort, and M. Kamps, Phys. Rev. Lett. **63**, 376 (1989).

[16] W. Barten, M. Lücke, and M. Kamps, in Ref. [17], p. 131.

[17] *Nonlinear Evolution of Spatio-Temporal Structures in Dissipative Continuous Systems*, Vol. 225 of *NATO Advanced Study Institue, Series B: Physics*, edited by F. H. Busse and L. Kramer (Plenum, New York, 1990).

[18] W. Barten, M. Lücke, M. Kamps, and R. Schmitz, Phys. Rev. E **51**, 5636 (1995).

[19] D. Bensimon, A. Pumir, and B. I. Shraiman, J. Phys. (France) **50**, 3089 (1989).

[20] St. Hollinger, P. Büchel, and M. Lücke, Phys. Rev. Lett. **78**, 235 (1997).

[21] E. Knobloch and D. R. Moore, in Ref. [17], p. 109.

[22] G. W. T. Lee, P. Lucas, and A. Tyler, J. Fluid Mech. **135**, 235 (1983).

[23] S. J. Linz and M. Lücke, Phys. Rev. A **35**, 3997 (1987); **36**, 2486(E) (1988).

[24] S. J. Linz, M. Lücke, H. W. Müller, and J. Niederländer, Phys. Rev. A **38**, 5727 (1988).

[25] W. Schöpf and W. Zimmermann, Phys. Rev. E **47**, 1739 (1993).

[26] G. Veronis, J. Mar. Res. **23**, 1 (1965).

[27] H. Yahata, Prog. Theor. Phys. Suppl. **99**, 493 (1989).

[28] O. Thual and S. Fauve, J. Phys. (France) **49**, 1829 (1988); B. A. Malomed and A. A. Nepomnyashchy, Phys. Rev. A **42**, 6009 (1990); W. van Saarloos and P. C. Hohenberg, Phys. Rev. Lett. **64**, 749 (1990); R. J. Deissler and H. R. Brand, Phys. Lett. A **146**, 252 (1990).

[29] H. Riecke, Phys. Rev. Lett. **68**, 301 (1992); Physica D **61**, 253 (1992); **92**, 69 (1996).

[30] Contrary to statements found in the literature the oscillatory instability is not caused by concentration diffusion being small: even if the diffusive time scales for momentum, heat, and concentration are the same ($L = \sigma = 1$) there are oscillations. They are caused by a sufficiently strong ''off diagonal'' Soret coupling between the degrees of freedom of concentration and temperature and their feedback into the buoyancy.

[31] P. Le Gal, A. Pocheau, and V. Croquette, Phys. Rev. Lett. **54**, 2501 (1985); E. Moses and V. Steinberg, Phys. Rev. A **43**, 707 (1991); M. A. Dominguez-Lerma, G. Ahlers, and D. S. Cannell, *ibid.* **52**, 6159 (1995).

[32] P. Bigazzi, S. Ciliberto, and V. Croquette, J. Phys. (France) **51**, 611 (1990); Ch. Jung, Ph.D. thesis, Universität des Saarlandes, Saarbrücken, Germany, 1997 (unpublished); B. Huke, Diploma thesis, Universität des Saarlandes, Saarbrücken, Germany, 1997 (unpublished).

[33] J. Liu and G. Ahlers, Phys. Rev. Lett. **77**, 3126 (1996).

[34] St. Hollinger and M. Lücke, Phys. Rev. E **57**, 4238 (1997).

[35] P. Büchel (private communication).

[36] M. C. Cross, Phys. Lett. A **119**, 21 (1986).

[37] G. Ahlers and M. Lücke, Phys. Rev. A **35**, 470 (1987).

[38] St. Hollinger, Ph.D. thesis, Universität des Saarlandes, Saarbrücken, Germany, 1996 (unpublished).

[39] St. Hollinger and M. Lücke, Z. Phys. B **103**, 531 (1997).

[40] W. Hort, S. J. Linz, and M. Lücke, Phys. Rev. A **45**, 3737 (1992).

[41] St. Hollinger and M. Lücke, Phys. Rev. E **52**, 642 (1995).

[42] E. N. Lorenz, J. Atmos. Sci. **20**, 130 (1963).

[43] O. Lhost, Ph.D. thesis, University of Mons, Belgium, 1990 (unpublished).

[44] J. Niederländer, M. Lücke, and M. Kamps, Z. Phys. B **82**, 135 (1991).

[45] St. Hollinger, Diploma thesis, Universität des Saarlandes, Saarbrücken, Germany, 1993 (unpublished).

[46] E. Knobloch, Phys. Rev. A **34**, 1538 (1986).